Original paper

The 2Q–(Or + Ab)–4An (QUORAA) diagram: poor for classification but good at deciphering the evolution of granitoids

Ming-ming SUN, Yang WANG*

School of Earth Sciences and Resources, China University of Geosciences (Beijing), Xueyuan Road 29, 100083 Beijing, P R China; e-mail: wangyang@cugb.edu.cn
**Corresponding author*

The 2Q–(Or + Ab)–4An (QUORAA) diagram (Enrique 2018) is proposed as an approximation of the modal QAP naming scheme for silica-saturated plutonic rocks. However, whether this scheme can reasonably reproduce the modal QAP classification results still needs to be tested. Through the inspection based on a dataset of 955 pairs of the mineral mode and whole-rock chemical compositions from the literature, it was found that the ratio of consistency between the two schemes is only 63.56 %. The consistency ratio is higher for discrimination of the granites (*s.s.*), but the inconsistency increases significantly for the rocks containing more mafic minerals (M > 25 %). As a section of the An–Ab–Or–Q (haplogranodiorite) tetrahedron, the QUORAA diagram is very helpful to illustrate the evolutionary paths of granitoid melts. The typical arc-related (ACG + ATG), the collision-related peraluminous (CPG + MPG), the rift-related peralkaline (PAG) as well as the potassic KCG granitoids show different trajectories in the QUORAA diagram. It is concluded that the QUORAA diagram would be applicable as a petrogenetic tool rather than the classification scheme.

Keywords: granitoid classification, petrogenetic tool, modal QAP diagram, 2Q–(Or + Ab)–4An diagram
Received: September 21, 2023; accepted: 22 January 2024; handling editor: V. Janoušek
The online version of this article (doi: 10.3190/jgeosci.388) contains supplementary electronic material.

1. Introduction

The classification is fundamental for the study of granitoids (Frost et al. 2001; Le Maitre 2002; Bonin et al. 2020). The modal QAPF scheme recommended by IUGS, whose purpose was to "give each plutonic rock its proper name" (Streckeisen 1976), has been widely accepted by the global geological community (Frost et al. 2019; Hogan 2019). Although the QAPF scheme is based on the objective mineral proportions (mode) of the plutonic and coarse-grained volcanic rocks, it suffers from the problem of dividing a continuum of rock compositions into several bins, because the mineral content of rocks in nature is gradually changing. Meanwhile, the point-counting of minerals in the thin-sections or slabs is time-consuming and boring. Or, worse still, it is imprecise or misleading, due to the presence of phenocrysts, fabric, problems with identification of colourless minerals etc. (Janoušek et al. 2014). Accordingly, the quantitative modal analyses of the granitoids are seldom reported in recent literature; for example, only about 5 % of the data in the igneous rock database in western North America (NAVDAT) reported its actual mineral contents (Glazner et al. 2019a, b).

Instead, a variety of schemes has been proposed to classify granitoids using petrochemical indicators (Le Maitre 1976; Streckeisen and Le Maitre 1979; Debon and Le Fort 1988; Middlemost 1994). However, there are contrasting opinions on the reliability of chemistry-based classification diagrams (Vilinovič and Petrík 1982; Whalen and Frost 2013; Stanley 2017; Bonin et al. 2020). Recently, Enrique (2018) proposed a new CIPW norm-based (Cross et al. 1902) 2Q–(Or + Ab)–4An diagram (abbreviated QUORAA below) for the classification of the silica-saturated plutonic rocks as an alternative of the QAP system. In the current paper, the reliability of the QUORAA scheme is tested by plotting a dataset of 955 pairs of mineral modes + whole-rock chemical compositions taken from the literature. The petrogenetic implications of the QUORAA diagram for granitoids are also discussed.

2. The QUORAA diagram

In the QAP scheme, three vertices Q, A, and P represent quartz, alkali feldspar and plagioclase respectively, and the silica-saturated plutonic rocks are classified into 17 categories according to the different Q–A–P portions (Fig. 1) (Streckeisen 1976; Le Maitre 2002). The QAP diagram is simple and reliable, making it very practical as a description and communication tool for naming granitoids (Bonin et al. 2020), but it does not apply to hypabyssal and volcanic rocks with fine mineral particles and/or glass. As pointed out by

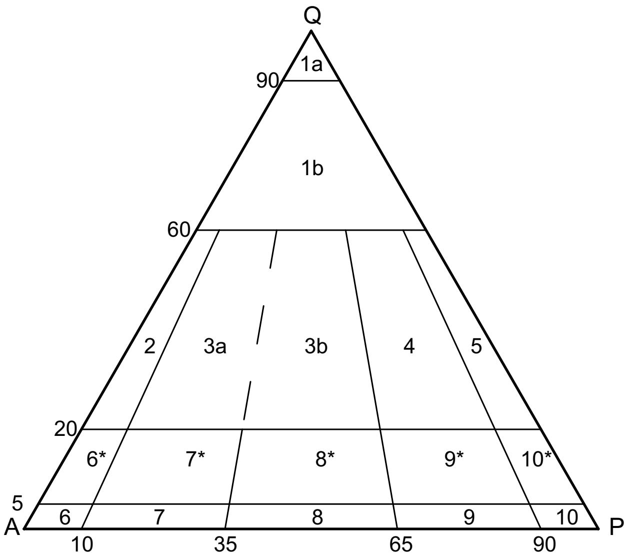

Fig. 1 The modal QAP ternary diagram (Streckeisen 1976). 1a quartzolite; 1b quartz-rich granitoid; 2 alkali-feldspar granite; 3 granite (3a syenogranite, 3b monzogranite); 4 granodiorite; 5 tonalite; 6* quartz alkali-feldspar syenite; 7*quartz syenite; 8* quartz monzonite; 9* quartz monzodiorite/quartz monzogabbro; 10* quartz diorite/quartz gabbro/quartz anorthosite; 6 alkali-feldspar syenite; 7 syenite; 8 monzonite; 9 monzodiorite/monzogabbro; 10 diorite/gabbro/anorthosite.

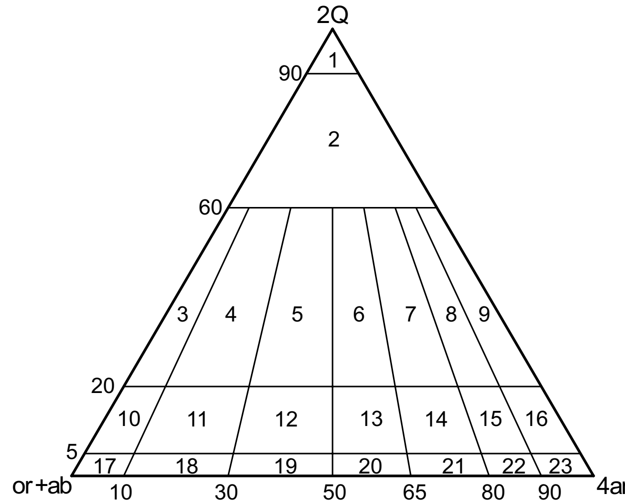

Fig. 2 The CIPW-normative 2Q–(Or+Ab)–4An (QUORAA) ternary diagram (Enrique 2018). 1 quartzolite, 2 quartz-rich granitoids, 3 alkali-feldspar granite, 4 syenogranite + sub-anorthite monzogranite, 5 monzogranite, 6 granodiorite, 7 tonalite, 8 tonalgabbro, 9 tonaleucrite, 10 quartz alkali-feldspar syenite, 11 quartz syenite, 12 quartz monzonite, 13 quartz monzodiorite/quartz monzogabbro, 14 quartz diorite, 15 quartz gabbro, 16 quartz eucrite, 17 alkali feldspar syenite, 18 syenite, 19 monzonite, 20 monzodiorite/monzogabbro, 21 diorite, 22 gabbro, 23 eucrite.

Enrique (2018), the QAP diagram cannot distinguish diorite with plagioclase An < 50 from gabbro with An ≥ 50 directly. Moreover, the QAP projection causes the discontinuous categorization of granites *(s.s.)* when the plagioclase falls below the 5 % of anorthite content, i.e., the projections of a continuum of granite (*s.s.*) compositions may jump from monzogranite to alkali feldspar granite.

Tab. 1 Compilation of literature sources that contain both the actual mineral modes and the whole-rock chemical compositions of plutonic rocks

Country	Plutons	Literature sources
Australia	Kosciusko Batholith (ACG+ATG, CPG+MPG)	Hine et al. (1978)
China	Beijing Badaling Batholith (KCG)	Bai et al. (1991)
China	The plutons of Hebei Province (KCG, TTG, PAG)	Wang et al. (1994)
Colombia	Ibagué Batholith (ACG+ATG)	Rodríguez-García et al. (2022)
Czech Republic	Central Bohemian Pluton (KCG)	Poubová (1974)
France	Margeride Pluton (CPG+MPG)	Debon and Le Fort (1988)
Norway	Lofoten–Vesteralen Batholith (PAG)	Malm and Ormaasen (1978)
Poland	Małopolska Batholith (ACG+ATG, KCG)	Wolska (2012)
Scotland, UK	Ballachulish Pluton (KCG, PAG)	Weiss and Troll (1989)
USA	Central Sierra Nevada plutons (ACG+ATG)	Bateman et al. (1984)
USA	Eastern Sierra Nevada and Benton Range plutons (ACG+ATG)	Bateman et al. (1984)
USA	Gibson Peak Batholith (ACG+ATG)	Lipman (1963)
USA	Marcy anorthosite–charnockite suite (PAG)	de Waard (1970)
USA	Mount Givens Granodiorite (ACG+ATG)	Bateman and Nokleberg (1978)
USA	Sherman Batholith (PAG)	Frost et al. (1999)
USA	Sierra National Forest plutons (ACG+ATG)	Bateman et al. (1984)
USA	South California Batholith (ACG+ATG)	Larson (1948)
USA	Tuolumne Intrusive Suite (ACG+ATG)	Bateman et al. (1988)
USA	White and Northern Inyo Mountains plutons (ACG+ATG)	Bateman et al. (1984)
USA	Yosemite plutons (ACG+ATG)	Bateman et al. (1984)

The abbreviations in the parentheses represent the Barbarin's (1999) granitoid groups each of batholiths/plutons belongs to. ACG – amphibole-rich calc-alkaline granitoids, ATG – arc "tholeiitic" granitoids, CPG – cordierite-bearing, biotite-rich peraluminous granitoids, MPG – muscovite-bearing peraluminous granitoids, KCG – K-rich and Kfs-phyric calc-alkaline granitoids, PAG – peralkaline and alkaline granitoids, TTG – tonalite, trondhjemite, granodiorite.

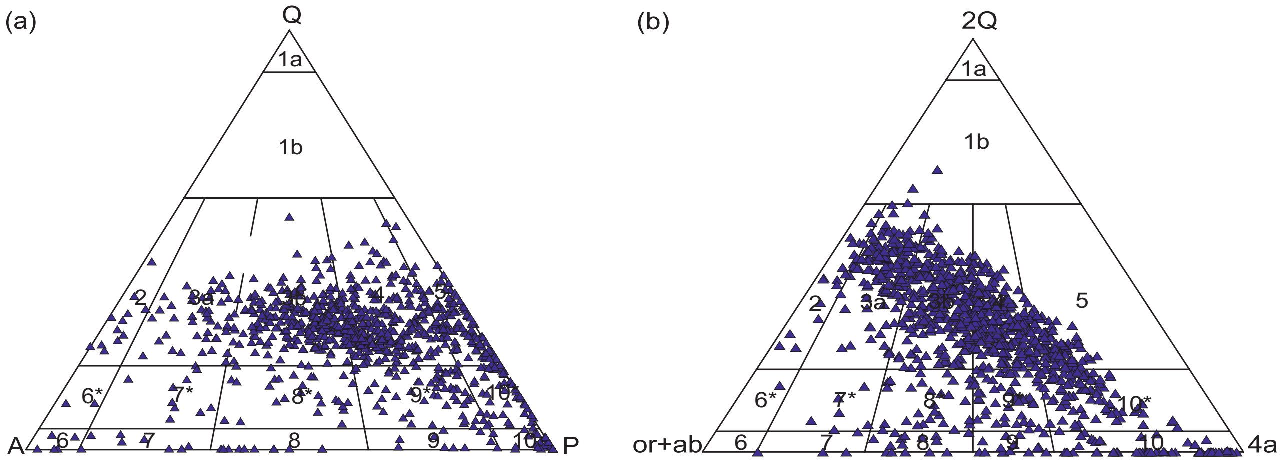

Fig. 3 The modal QAP (a) and CIPW-normative QUORAA (b) ternary diagrams for all 955 analyses compiled from the literature (the data sources are shown in Table 1).

The QUORAA scheme is proposed to overcome the shortcomings of the QAP scheme mentioned above (Enrique 2018). In this new, CIPW norm-based diagram, the silica-saturated plutons are classified into 23 fields according to the ternary feldspar index IFT = 100 × An/(An + Ab + Or) (Fig. 2). The apices of the ternary diagram are CIPW-normative 2 × Qz, (Or + Ab), and 4 × An, respectively.

Enrique (2018) believed that the QUORAA scheme realizes the uninterrupted classification of silica-saturated igneous rocks, keeping most of the same naming as the QAP classification system. Compared with the QAP diagram, its merits include that:

1) After the combination of CIPW-normative Ab and Or as one apex, it demonstrates the progressive evolution of the feldspar series from the calcic to the sodic plagioclase and the K-feldspar. This treatment removes the jumps caused by the distinction of the albite with An < 5 from the plagioclase with An > 5.
2) The overlap between diorite and gabbro is avoided.
3) Using the CIPW norm, the new scheme is more convenient in practice than the point-counting procedure, and it can be applied consistently to the hypabyssal and volcanic rocks as well.

3. Reliability test for the QUORAA scheme

3.1. Data compilation and projections

For testing the reliability of the QUORAA scheme, 955 data pairs from samples for which were available both a mineral mode and a chemical composition were projected in the modal QAP and the normative QUORAA diagrams, respectively (Fig. 3). The data are compiled from the literature (see Tab. 1 for sources).

To remove the potential bias from using the different CIPW norm calculation procedures, all chemical data were calculated by the CIPW norm software SINCLAS (Verma et al. 2002), applying the adjustment of iron oxides proposed by Middlemost (1989).

For the convenience of comparison, the categories in QUORAA diagram are matched with the fields of QAP classification system (Tab. 2 and Fig. 3). The actual mineral modes of each sample in the compilation are projected in the QAP diagram; at the same time, the corresponding CIPW norms are plotted in the QUORAA diagram. When the rock names from QAP and QUORAA

Tab. 2 Correspondence between the categories/fields of the QAP and the QUORAA diagrams

QAP fields	QUORAA categories
1a Quartzolite	*1 Quartzolite*
1b Quartz-rich granitoids	*2 Quartz-rich granitoids*
2 Alkali-feldspar granite	*3 Alkali-feldspar granite*
3 Granite	*4 Syenogranite + sub-anorthite monzogranite, 5 Monzogranite*
4 Granodiorite	*6 Granodiorite*
5 Tonalite	*7 Tonalite, 8 Tonalgabbro, 9 Tonaleucrite*
6* Quartz alkali-feldspar syenite	*10 Quartz alkali-feldspar syenite*
7* Quartz syenite	*11 Quartz syenite*
8* Quartz monzonite	*12 Quartz monzonite*
9* Quartz monzodiorite	*13 Quartz monzodiorite/Quartz monzogabbro*
10* Quartz diorite/Quartz gabbro	*14 Quartz diorite, 15 Quartz gabbro, 16 Quartz eucrite*
6 Alkali feldspar syenite	*17 Alkali feldspar syenite*
7 Syenite	*18 Syenite*
8 Monzonite	*19 Monzonite*
9 Monzodiorite	*20 Monzodiorite/Monzogabbro*
10 Diorite/Gabbro/Anorthosite	*21 Diorite, 22 Gabbro, 23 Eucrite*

The rock names for each QAP field and QUORAA category are taken from Le Maitre (2002) and Enrique (2018), respectively. The category numbers and rock names of the QUORAA diagram are listed in italics.

Tab. 3 Replication rates of the QUORAA discrimination (correspondence to the QAP fields) (sample size ≥ 10)

QAP fields	QUORAA categories	Sample size	Replication rate (%)
2 Alkali-feldspar granite	3	12	50.00
3 Granite	4, 5	322	82.92
4 Granodiorite	6	291	60.14
5 Tonalite	7, 8, 9	121	47.11
8* Quartz monzonite	12	26	30.77
9* Quartz monzodiorite	13	59	42.37
10* Quartz diorite/Quartz gabbro	14, 15, 16	67	55.32
8 Monzonite	19	11	63.64
9 Monzodiorite	20	10	60.00
10 Diorite/Gabbro/Anorthosite	21, 22, 23	32	84.38

diagrams match, the sample is counted as "right" (1); if not, it is counted as wrong (0). The final scores (replication rates) of the QUORAA diagram are derived from the number of samples that fell in the "right" fields of QAP scheme.

3.2. Results

Using the compiled literature dataset, 608 samples out of the 955 plot into the consistent categories in both diagrams (Fig. 3). This means that the QUORAA diagram replicates the modal QAP classifications at a rate of 63.56 % for the compiled dataset.

More detailed QUORAA discrimination results for the individual categories of modal QAP are listed in Tab. 3. The replication rates for granite (*s.s.*) (Field 3) and diorite (Field 10) are more than 80 %. For the samples belonging to the granodiorite (Field 4), monzonite (Field 8), and monzodiorite (Field 9) fields in the modal QAP diagram, the QUORAA diagram gets replication rates of 60 %. Moreover, it is unsuccessful to discriminate the tonalite (Field 5), quartz monzonite (Field 8*), and quartz monzodiorite (Field 9*). For the same QAP categories, the replication rates of the felsic samples (M < 25 %) are higher than those of the more mafic ones (M > 25 %) ones with the exception of the diorite rocks (fields 10* and 10) (Tab. 4).

Tab. 4 Replication rates of the QUORAA discrimination (correspondence to the QAP fields) with variable modal contents of mafic minerals (M)

QAP categories	M > 25 vol. %	Replication rate (%)	M < 25 vol. %	Replication rate (%)
2 Alkali-Fsp granite	–	–	12	50.00
3 Granite	3	33.33	303	83.50
4 Granodiorite	11	54.55	279	60.57
5 Tonalite	31	35.48	90	52.22
8* Qtz monzonite	2	0.00	24	33.33
9* Qtz monzodiorite	14	28.57	43	46.51
10* Quartz diorite	28	71.43	19	31.58
8 Monzonite	1	0.00	10	70.00
9 Monzodiorite	5	60.00	5	60.00
10 Diorite/Gabbro	28	85.71	4	75.00
Total	123	55.65	789	64.66

M – volume percentage of the mafic and related minerals in the rock (see Le Maitre 2002, p. 4 for definition).

The replication rates of the QUORAA diagram vary from case to case. The S-type granitoids of Kosciusko Batholith in Australia (20 samples) have a success discrimination rate of 85 %, compared with the modal QAP classification (Fig. 4a–b). For the eighty-two samples of the Early Yanshanian (Jurassic) plutons from Hebei Province, China, fifty-three samples are correctly discriminated by QUORAA diagram (~65% success rate) (Fig. 5a–b). The QUORAA diagram does not yield acceptable results for the 13 samples from the Małopolska Batholith of Poland (Fig. 6a–b), as the projections of six host granite samples are shifted from the tonalite (Field 5) and granodiorite (Field 4) of the modal QAP diagram to the granodiorite (Field 4) and granite (fields 3a and 3b) within the QUORAA diagram. In contrast, the mafic microgranular enclaves (MMEs) (14 samples) jump from the tonalite (Field 5) and quartz diorite (Field 10*) to the granodiorite (Field 4) and quartz monzodiorite (Field 9*).

4. Discussion

The two thirds replication rate of 955 modal–chemical pairs of granitoids implies that the recently proposed QUORAA scheme does not work satisfactorily to classify granitoids. Especially, the QUORAA diagram performs poorly for discrimination of tonalite, quartz diorite, quartz monzonite, and quartz monzodiorite (in the sense of modal QAP) (Tab. 3). Many projection points within the QUORAA diagram are shifted leftwards or left-downwards compared to the original positions within the modal QAP diagram (Figs 3–6), while the those plotting near the left edge of the modal QAP triangle move upwards in the QUORAA diagram (Figs 3 and 5). Accordingly, the QUORAA diagram should not be used as a proxy of the modal QAP scheme for the classification and nomenclature of the granitoid rocks (*s. l.*). It is also suspected whether the QUORAA scheme could be applied successfully to the hypabyssal and eruptive rocks as the original article of Enrique (2018) suggested.

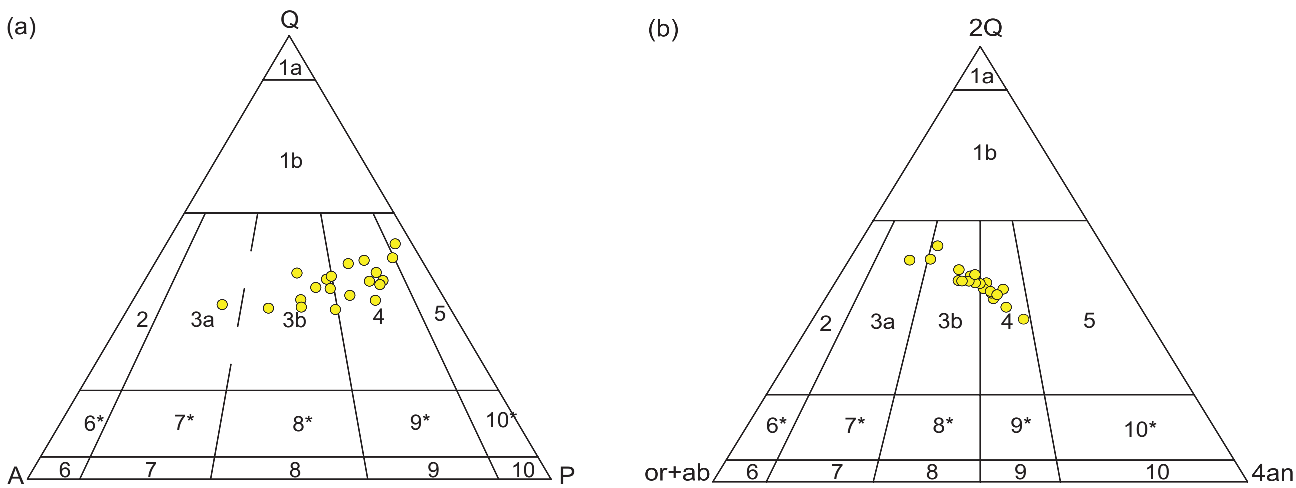

Fig. 4 The modal QAP (a) and CIPW-normative QUORAA (b) ternary diagrams for the S-type granitoids, Kosciusko Batholith, Australia (data from Hine et al. 1978).

Although chemical classifications of igneous rocks can generally match the results of the modal QAP scheme, their reliability is still debated (Vilinovič and Petrík 1982; Stanley 2017; Bonin et al. 2020). Bonin et al (2020) pointed out that the presence of biotite causes an increase in CIPW-normative orthoclase (Or) and a decrease in CIPW-normative quartz (Q) compared with the modal proportions of the same minerals in the actual rocks. Therefore, projection points of biotite-rich rocks may be shifted significantly towards the left or left-down side of the QUORAA diagram. Biotite may be the dominant mafic mineral in many igneous rocks, e.g., tonalites, granodiorites, quartz diorites as well as diorites. This fact explains why the QUORAA diagram performs poorly for tonalites and quartz diorites. This problem could be overcome by using the Mesonorm instead of the CIPW norm for the projection (Vilinovič and Petrík 1982).

The weight of quartz in the 2Q apex of the QUORAA triangle is two times that of alkali-feldspars, thus the projection points of the alkali feldspar syenite and the quartz alkali feldspar syenite (i.e., of sodic plagioclase- and K-feldspar-rich rocks) may move towards the 2Q apex. In these cases, the weight of CIPW-normative quartz vertex overcomes the CIPW-normative Q decrease induced by biotite as mentioned above.

It is attractive that most points within the QUORAA diagram project along a negative trend from the 4An vertex towards the middle of the 2Q–(Or + Ab) edge (e.g., Fig. 3b). This trend is also explicitly exhibited on the batholith scale. The typical examples include the South California, Tuolumne, Ballachulish, and Lofoten–Vesteralen batholiths (Fig. 7). Another two examples are shown in Fig. 4 (S-type granitoids of Kosciusko Batholith, Australia) and Fig. 5 (Early Yanshanian intrusive rock samples of Hebei Province, China).

This negative trend ends roughly in the middle of the 2Q–(Or + Ab) side, which corresponds to the normative proportion of Q to (Or + Ab) ≈ 1 : 2. Assuming a ratio of

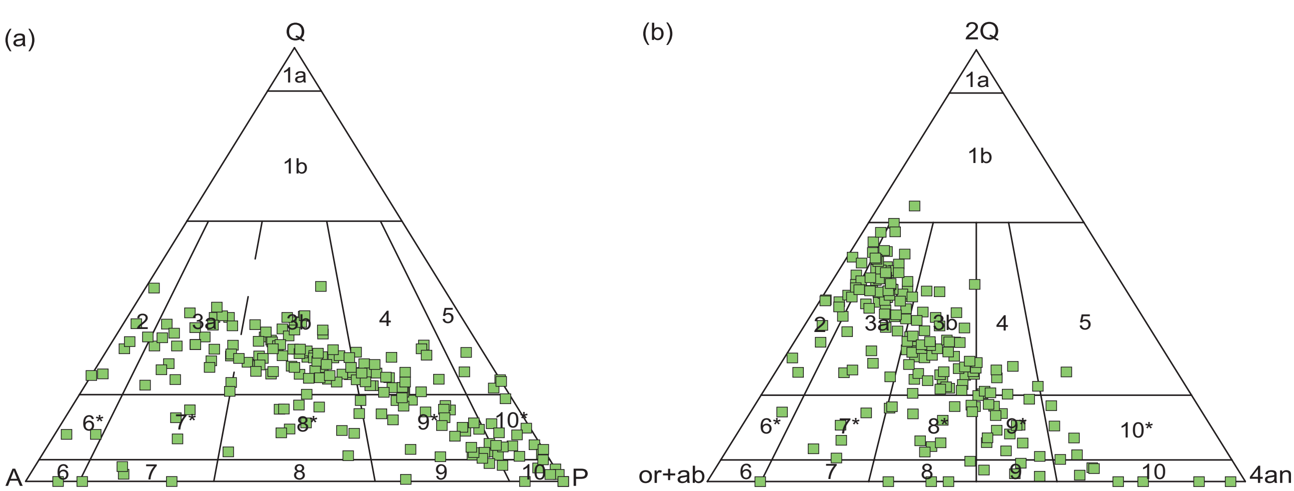

Fig. 5 The modal QAP (a) and CIPW-normative QUORAA (b) ternary diagrams for the Early Yanshanian intrusive rocks in Hebei Province, China (data from Wang et al. 1994).

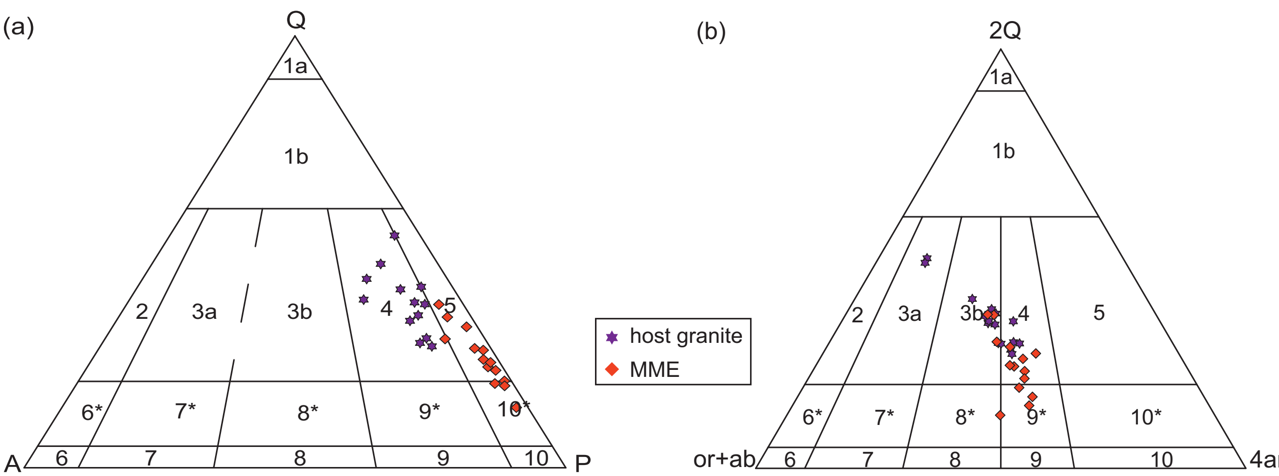

Fig. 6 The modal QAP (a) and CIPW-normative QUORAA (b) ternary diagrams for the mafic enclaves (MMEs) and the host granite of Małopolska Batholith, Poland (data from Wolska 2012).

Or : Ab ≈ 1 : 1, the middle of the 2Q–(Or + Ab) side is close to the thermal minimum of the haplogranite–H_2O system under low-pressure conditions (Q : Or : Ab ≈ 1 : 1 : 1) (Tuttle and Bowen 1958). Accordingly, this negative trend end in the QUORAA diagram demonstrates the successive evolution of granitoid associations from the dioritic end-member to the eutectic or thermal minimum point of granite (*s.s.*).

In fact, the QUORAA triangular diagram may be considered as a sectional drawing of the An–Ab–Or–Q tetrahedron (a.k.a. haplogranodiorite system) (Fig. 8, Luth 1976). Two distinct evolutionary paths can be distinguished for different primitive melts.

The Si-poor and Ca-rich primitive melt (projection close to the An vertex of haplogranodiorite tetrahedron) evolves towards the Q–An–Ab–Or (quartz–feldspars) cotectic surface (e1–e2–e3 surface in Fig. 8). After reaching it, the residual melt follows the cotectic plane towards the eutectic (higher pressure) or thermal minimum (lower pressure) point of the Ab–Or–Q section (i.e., the haplogranite system). Along this evolutionary path, the compositions of evolved melts are constrained by the coeval crystallization of quartz and feldspars, forming a left-upwards trend in the QUORAA diagram.

On the contrary, the Si- and Ca-poor primitive melt (projection near the Or–Ab side) may firstly evolve towards the cotectic surface e4–E2–E1–e5 by fractionation of Or (when Or content exceeds that of Ab). After then, the residual melt composition follows the plane towards the quartz–feldspars cotectic surface. Finally, the melts differentiate towards the eutectic or thermal minimum point of the Ab–Or–Q section along the cotectic line E2–E1.

Actually, these two different paths result from fractionation dominated, respectively, by calcic plagioclase (projecting as 4An), or by alkali feldspars (projecting as Or + Ab) in the QUORAA ternary.

Four characteristic plutonic rock types are identified in the QAP diagram, i.e. (1) the tholeiitic series, deprived

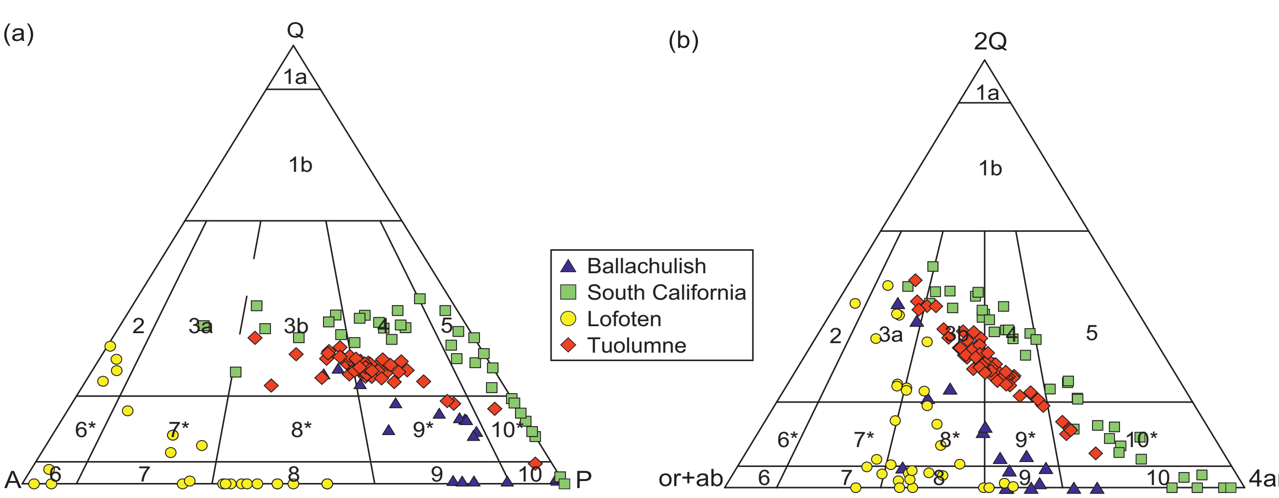

Fig. 7 The QAP (a) and QUORAA (b) ternary diagrams of the typical alkaline, alkali-calcic, calc-alkaline, and calcic series (the data sources are shown in Tab. 1).

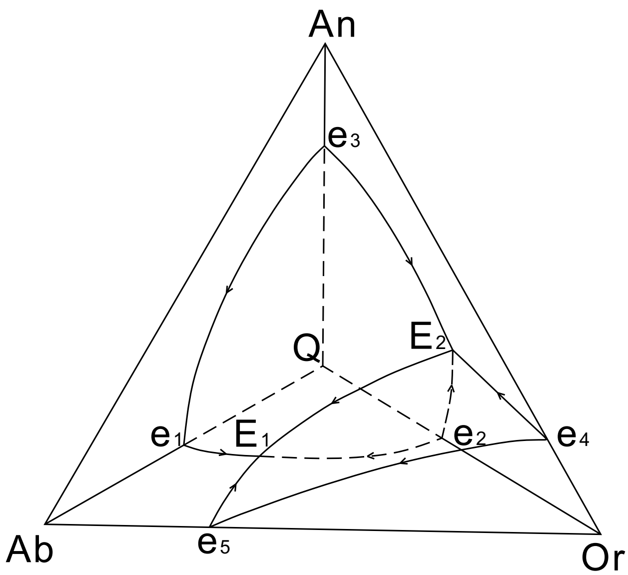

Fig. 8 Schematic phase diagram of the haplogranodiorite–H_2O system (modified from Luth 1976, fig. 20).

of K feldspars, (2) the calc-alkaline series, (3) the alkaline series with its characteristic syenitic members, and (4) quartz-rich granitoids (Lameyre and Bowden 1982; Lameyre and Bonin 1991). Enlighted by the insight of Lameyre and co-workers, we projected the compositions of calcic (South California, Larson 1948), calc-alkalic (Tuolumne, Bateman et al. 1988), alkali-calcic (Ballachulish, Weiss and Troll 1989), and alkalic (Lofoten–Vesteralen, Malm and Ormaasen 1978) granitoid series (Frost et al. 2001; Frost and Frost 2008) within the modal QAP and the QUORAA diagrams (Fig. 7a–b). In the QUORAA diagram, the calcic South California and the calc-alkalic Tuolumne Batholith display linear evolutionary trends from diorite/gabbro end-member to granodiorite and monzogranite fields, and terminate in the syenogranite field. The alkali-calcic Ballachulish rocks evolve from monzodiorite to granite (*s.s.*). The plots of the alkalic Lofoten–Vesteralen Batholith spread from the monzonite/syenite to the quartz monzonite/quartz syenite fields, and end in the syenogranite and the alkali-feldspar granite fields. It is obvious that the calcic and the calc-alkalic granitoids evolve along the first path within the haplogranodiorite tetrahedron; however, alkali-calcic and alkalic granitoids evolve along the second path distinguished above.

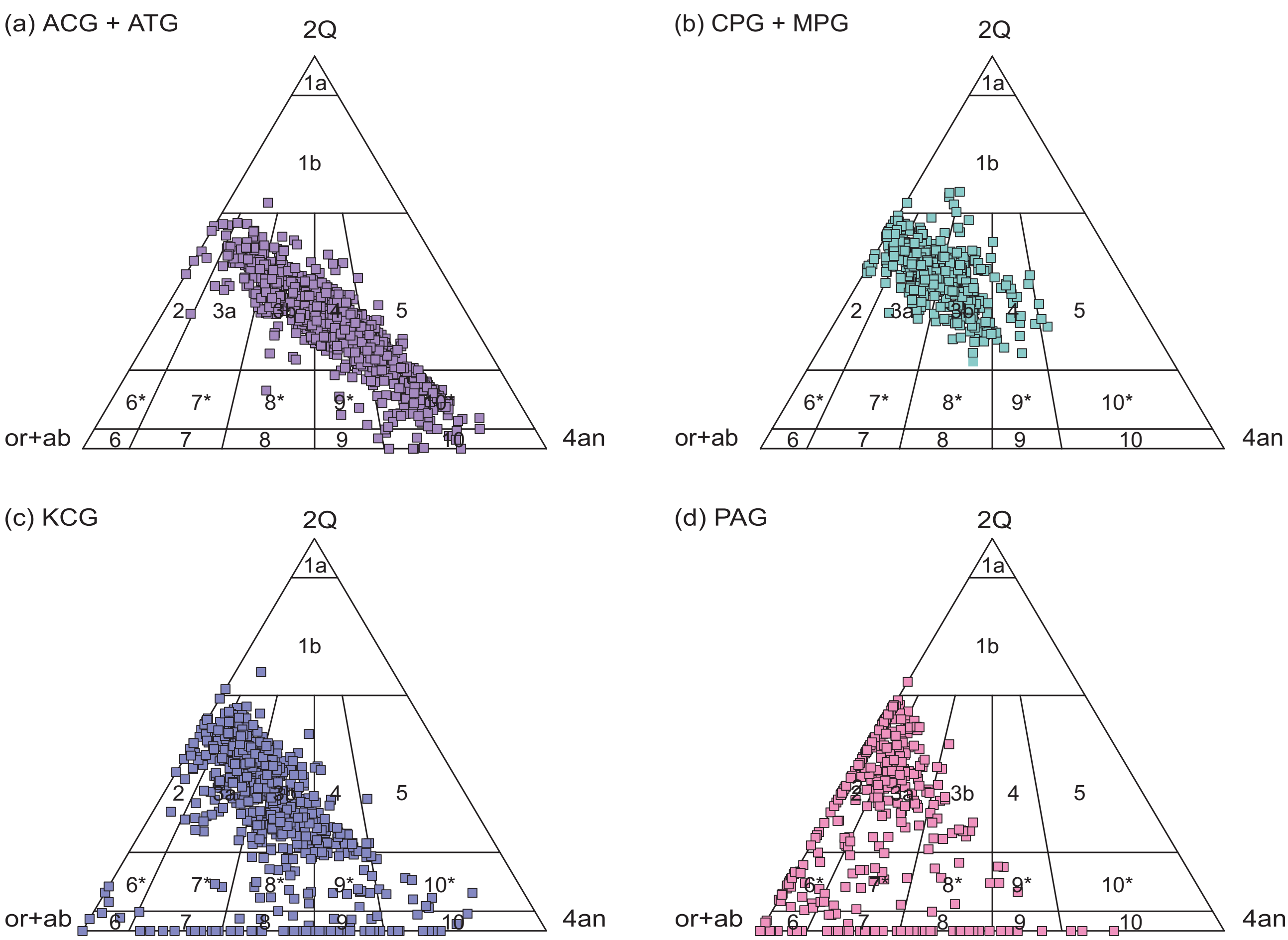

Fig. 9 The QUORAA ternary diagram of (a) ACG + ATG; (b) CPG and MPG; (c) KCG; (d) PAG (data from Bonin et al. 2020).

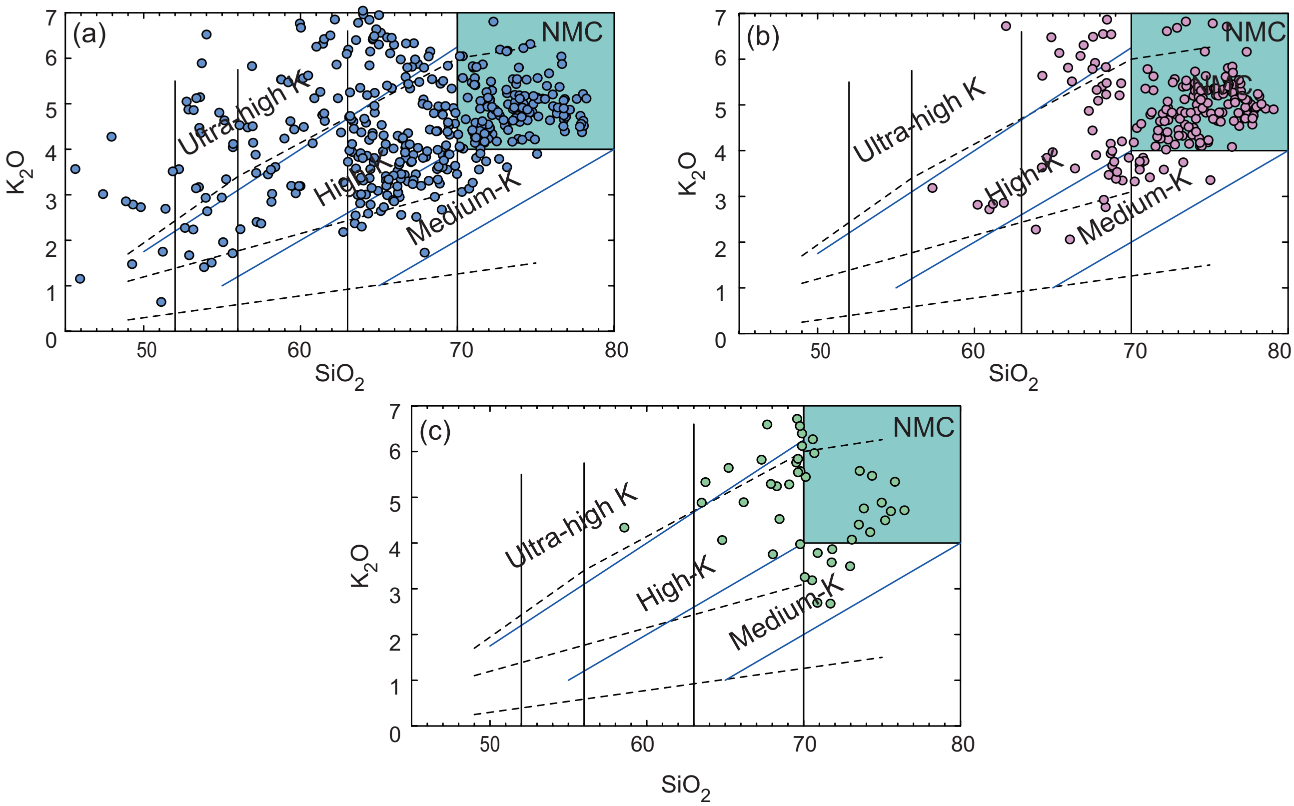

Fig. 10 The SiO_2 vs. K_2O diagram of **(a)** metaluminous (ACNK < 1) KCG; **(b)** weakly peraluminous (1 < ACNK < 1.1) KCG and **(c)** strongly peraluminous (ACNK > 1.1) KCG (data from Bonin et al. 2020). The solid lines between different potassic series are replicated from Jacob et al. (2021), and the dashed lines are those of Peccerillo (2017). NMC: near-minimum melt compositions.

Barbarin (1999) defined granitoid groups based on characteristic minerals and major-element chemistries as: ACG – amphibole-rich calc-alkaline granitoids, ATG – arc "tholeiitic" granitoids, CPG – cordierite-bearing, biotite-rich peraluminous granitoids, MPG – muscovite-bearing peraluminous granitoids, KCG – K-rich and Kfs-phyric calc-alkaline granitoids, PAG – peralkaline and alkaline granitoids, RTG – ridge "tholeiitic" granitoids (plagiogranites).

The ACG and ATG group corresponds to the primary I-type granites as defined by Castro (2020), whereas PAGs are peralkaline, rift-related granitoids. In general, ACG + ATG and PAG rocks are dominantly generated through the crystallization of a more primitive melt (Bonin 2007; Castro 2020; Moyen et al. 2021). However, the CPG + MPG group corresponds to S-type granites in a broad sense, and as such are the product of crustal melting (Nabelek 2020; Moyen et al. 2021). The KCG group (Bonin et al. 2020) may be assigned to the secondary I-type granites of Castro (2020) due to their hybrid genesis.

We applied the QUORAA diagram to the typical ACG + ATG, CPG + MPG, KCG, and PAG datasets from Bonin et al (2020) (Fig. 9). The arc granitoids (ACG + ATG) display a "perfect" linear trend from the diorite corner to the middle of the 2Q–(Or + Ab) edge (eutectic composition of haplogranite) (Fig. 9a). The peralkaline granites (PAG) spread over the fields in the left half, close to the (Or + Ab) apex (Fig. 9d). Data points along the bottom side indicate that some PAG magmas evolve along the second path within the haplogranodiorite tetrahedron. The ATG + ACG and the PAG assemblages represent two end-member differentiation trends of granitoids (see also Whalen and Frost 2013).

The peraluminous CPG + MPG group also evolves to the upper left, but lacks the mafic members such as diorite/quartz diorite, being mainly distributed within the syenogranite and monzogranite fields (Fig. 9b).

The KCGs are described as "worst-defined group" by Bonin et al. (2020), and this is obviously reflected also by the QUORAA diagram (Fig, 9c). For getting more consistent trends, the KCGs are sub-grouped according to their peraluminosity (ACNK ratio) and K_2O content (Figs 10, 11). The majority of KCGs belong to metaluminous (ACNK < 1) sub-group (Fig. 10a), and the weakly peraluminous (1 < ACNK < 1.1) samples are subordinate (Fig. 10b), meanwhile the strongly peraluminous ones (ACNK > 1.1) are rare (Fig. 10c). The metaluminous KCGs focus around the monzogranite field, and some are rooted within quartz-poor fields such as diorite, monzodiorite, and monzonite (Fig. 11a). Meanwhile many "ultra-high

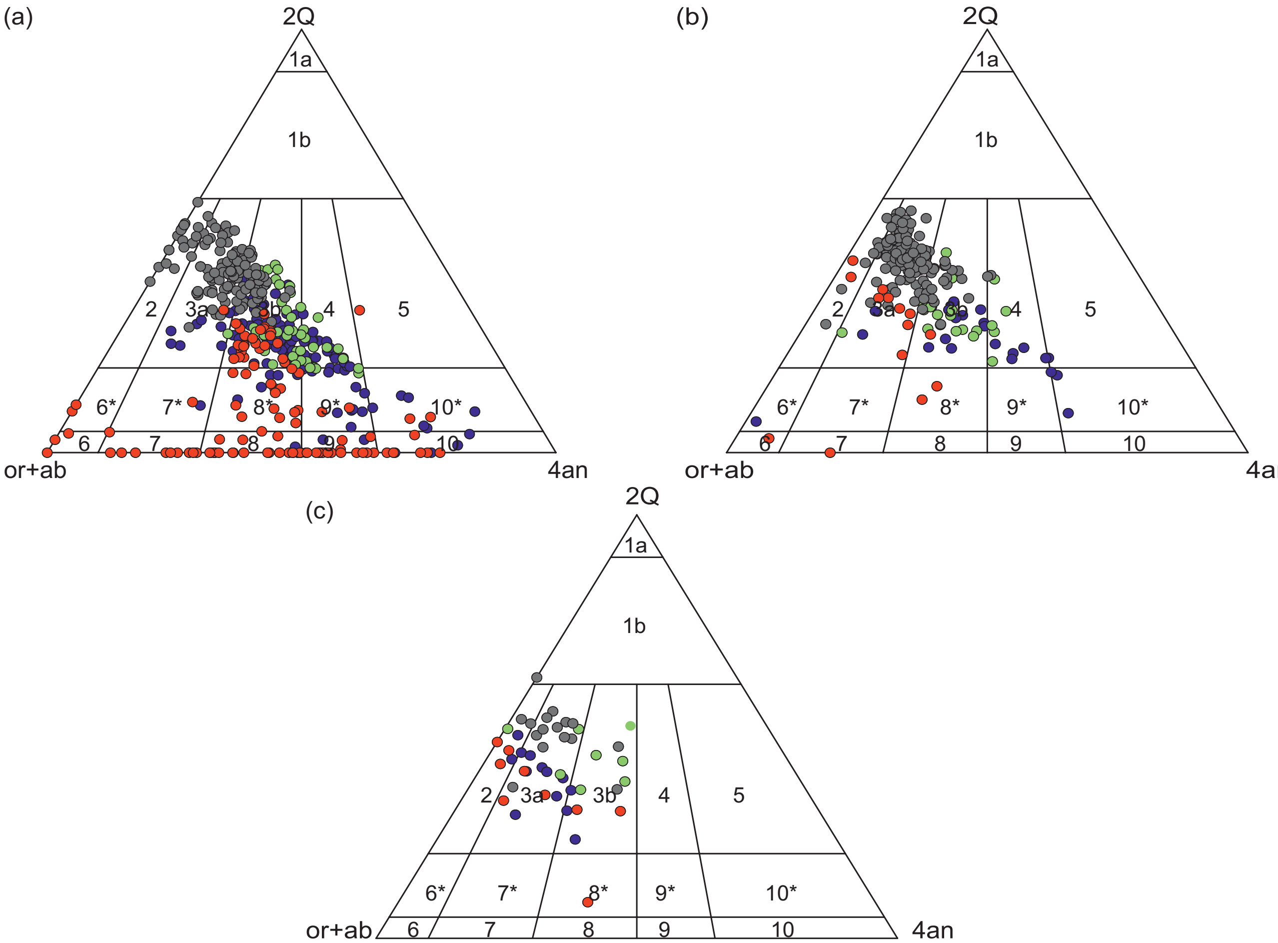

Fig. 11 The QUORAA ternary diagram of **(a)** metaluminous (ACNK < 1) KCG; **(b)** weakly peraluminous (1 < ACNK < 1.1) KCG and **(c)** strongly peraluminous (ACNK > 1.1) KCG (data from Bonin et al. 2020). The samples in red are "ultra-high K", the blue ones are "high-K", the green ones "median-K", and the grey ones are near-minimum melt compositions (NMC) as discriminated in Figure 10. ACNK: $Al_2O_3/(CaO + Na_2O + K_2O)$, molar ratio.

K" as well as some "high-K" metaluminous KCGs spread along the bottom of QUORAA ternary, corresponding to the differentiation path of basic PAGs. Most of the peraluminous KCGs fall in the syenogranite/alkali-feldspar granite categories of QUORAA diagram (Fig. 11b–c), and resemble the pattern of the CPG + MPG group.

In the SiO_2 vs. K_2O diagram, a significant portion of basic metaluminous KCGs falls in "ultra-high K" domain (Fig. 10a). In contrary, almost all "ultra-high K" peraluminous samples are acid with SiO_2 content more than 63 % (Fig. 10b, c). The distinct patterns of the KCG sub-groups in QUORAA diagram imply the different petrogenesis of these rocks. The peraluminous KCGs can be regarded as the "hybrids" of the evolved mafic magma and the crust-derived K-rich sources as suggested by Castro (2020). However, the low-silica "ultra-high K" metaluminous KCGs crystallized from the K-rich parental magmas generated by the melting of metasomatic mantle (Förster et al. 2020). Accordingly, these low-silica "ultra-high K" rocks should be separated from the KCG as a distinct group (shoshonite association) following the suggestions of Joplin (1965, 1968, 1971).

In summary, plotting of the compositions of plutonic rocks in the QUORAA diagram underlines variations among different magma series/associations/groups. The evolution of a specific suite may be deduced by the comparison of its projection with those of typical granitoid series. At the same time, the likely source composition (rich in calcic plagioclase or alkali feldspar) might be inferred from the compositional evolution path in the QUORAA diagram. Therefore, the QUORAA plot seems helpful to better understanding the genesis of granitoid rocks.

5. Conclusions

By a compilation of 955 pairs of measured mineral modes and major-element compositions, we checked the reliability of the QUORAA diagram as an approximation of the modal QAP scheme for naming the common plutonic rocks, and the results show that:

1) The QUORAA diagram assigns *c.* 64 % of samples into the "correct" categories of the modal QAP scheme. With a replication rate of over 80 %, the discrimination of granite (*s.s.*) by QUORAA diagram is acceptable in practice. But this diagram performs poorly in distinguishing the tonalite and quartz diorite with a replication rate of less than 60 %. Therefore, the QUORAA scheme might not be a good approximation of the modal QAP scheme for granitoid classification and nomenclature, and is probably not suitable for the hypabyssal or volcanic rocks, either.
2) As a section of the An–Ab–Or–Q tetrahedron (haplogranodiorite system), the QUORAA diagram is very helpful to illustrate differentiation of granitoid melts. The typical calc, calc-alkalic, alkalic-calc, and alkalic granitoid series display contrasting paths/fall into distinct fields within the QUORAA diagram.
3) The arc (ACG + ATG) and the peralkaline (PAG) granitoids evolve along two different crystallization paths, which are easily distinguished in the QUORAA diagram. The potassic granitoids (KCG) are derived from hybrid processes as suggested by their "transitional" position within the QUORAA diagram. Taken together, the QUORAA diagram seems applicable as a petrogenetic tool rather than a classification scheme.

Acknowledgements. Trond Slagstad from the Norwegian Geological Survey (NGU) kindly provided the electronic literature of the Lofoten–Vesteralen Batholith. Detailed and constructive reviews by Bernard Bonin, Igor Petrík, and editor Vojtěch Janoušek improved the paper significantly.

Electronic supplementary material. Supplementary table of the compilation of granitoids with whole-rock chemistry and actual QAP mode is available online at the Journal web site (*http://dx.doi.org/10.3190/jgeosci.388*).

References

Bai Z, Xu S, Ge S (1991) Badaling Magmatic Complex. Geological Publishing House, Beijing, pp 1–169 (in Chinese)

Barbarin B (1999) A review of the relationships between granitoid types, their origins and their geodynamic environments. Lithos 46: 605–626

Bateman PC, Nokleberg WJ (1978) Solidification of the Mount Givens granodiorite, Sierra Nevada, California. J Geol 86: 563–579

Bateman PC, Dodge FCW, Bruggman PE (1984) Major oxide analyses, CIPW norms, modes, and bulk specific gravities of plutonic rocks from the Mariposa 1° × 2° sheet, central Sierra Nevada, California. USGS Open-File Report 84–162, pp 1–50

Bateman PC, Chappell BW, Kistler RW, Peck DL, Busacca A (1988) Tuolumne Meadows Quadrangle, California – Analytic Data. USGS Bulletin 1819, pp 1–43

Bonin B (2007) A-type granites and related rocks: evolution of a concept, problems and prospects. Lithos 97: 1–29

Bonin B, Janoušek V, Moyen J-F (2020) Chemical variation, modal composition and classification of granitoids. In: Janoušek V, Bonin B, Collins WJ, Farina F, Bowden P (eds) Post-Archaean Granitic Rocks: Contrasting Petrogenetic Processes and Tectonic Environments. Geological Society, London, Special Publications 491: 9–51

Castro A (2020) The dual origin of I-type granites: the contribution from laboratory experiments. In: Janoušek V, Bonin B, Collins WJ, Farina F, Bowden P (eds) Post-Archaean Granitic Rocks: Contrasting Petrogenetic Processes and Tectonic Environments. Geological Society, London, Special Publications 491: 101–145

Cross W, Iddings JP, Pirsson LV, Washington S (1902) A quantitative chemico–mineralogical classification and nomenclature of igneous rocks. J Geol 10: 555–690

Debon F, Le Fort P (1988) A cationic classification of common plutonic rocks and their magmatic associations: principles, method, applications. Bull Minéral 111: 493–510

de Waard D (1970) The anorthosite–charnockite suite of rocks of Roaring Brook Valley in the eastern Adirondacks (Marcy Massif). Amer Miner 55: 2063–2075

Enrique P (2018) Clasificación normativa de las rocas plutónicas saturadas y sobresaturadas en sílice basada en la clasificación modal QAP: el diagrama 2Q–(or+ab)–4an. Geogaceta 63: 95–98

Förster MW, Buhre S, Xu B, Purelecić D, Mertz-Kraus R, Foley SF (2020) Two-stage origin of K-enrichment in ultrapotassic magmatism simulated by melting of experimentally metasomatized mantle. Minerals 10: 41

Frost BR, Frost CD (2008) A geochemical classification for feldspathic igneous rocks. J Petrol 49: 1955–1969

Frost CD, Frost BR, Chamberlain KR, Edwards BR (1999) Petrogenesis of the 1.43 Ga Sherman Batholith, SE Wyoming, USA: a reduced, rapakivi-type anorogenic granite. J Petrol 40: 1771–1802

Frost BR, Barnes CG, Collins WJ, Arculus RJ, Ellis DJ, Frost CD (2001) A geochemical classification for granitic rocks. J Petrol 42: 2033–2048

Frost BR, Frost CD, Anderson LA, Barens CG, Wilson BM (2019) A more informative way to name plutonic rocks – Comment by Frost et al. GSA Today 29: DOI 10.1130/GSATG405C.1

Glazner AF, Bartley JM, Coleman DS (2019a) A more informative way to name plutonic rocks. GSA Today 29: 4–10

Glazner AF, Bartley JM, Coleman DS (2019b) A more informative way to name plutonic rocks – Reply. GSA Today 29: DOI 10.1130/GSATG408Y.1

Hine R, Williams IS, Chappell BW, White AJR (1978) Contrasts between I- and S-type granitoids of the Kosciusko Batholith. J Geol Soc, Australia 25: 219–234

Hogan P (2019) A more informative way to name plutonic rocks – comment by Hogan. GSA Today 29: DOI 10.1130/GSATG406C.1

Jacob J-B, Moyen J-F, Fiannacca P, Laurent O, Bachmann O, Janoušek V, Farina F, Villaros A (2021) Crustal melting vs. fractionation of basaltic magmas: Part 2, Attempting to quantify mantle and crustal contributions in granitoids. Lithos 402–403: 106292

Janoušek V, Navrátil T, Trubač J, Strnad L, Laufek F, Minařík L (2014) Distribution of elements among minerals of a single (muscovite-) biotite granite sample - an optimal approach and general implications. Geol Carpath 65: 257–271

Joplin GA (1965) The problem of the potash-rich basaltic rocks. Min Mag 65: 266–374

Joplin GA (1968) The shoshonite association: a review. J Geol Soc Aust 15: 275–294

Joplin GA (1971) A Petrography of Australian Igneous Rocks, Including Material from the Territory of Papua and New Guinea (Revised Edition). Angus and Robertson, Sydney, pp 1–25

Lameyre J, Bonin B (1991) Granites in the main plutonic series. In: Didier J, Barbarin B (eds) Enclaves and Granite Petrology. Elsevier, Amsterdam, pp 3–17

Lameyre J, Bowden P (1982) Plutonic rock types series: discrimination of various granitoid series and related rocks. J Volcanol Geotherm Res 14: 169–186

Larson ES (1948) Batholith and associated rocks of Corona, Elsinore, and San Luis Rey quadrangles southern California. GSA Memoir 29, pp 1–175

Le Maitre RW (1976) Some problems of the projection of chemical data into mineralogical classifications. Contrib Mineral Petrol 56: 181–189

Le Maitre RW (ed.) (2002) Igneous Rocks: A Classification and Glossary of Terms (2nd ed). Cambridge University Press, Cambridge, pp 1–236

Lipman PW (1963) Gibson Peak Pluton: a discordant composite intrusion in the southeastern Trinity Alps, northern California. GSA Bulletin 74: 1259–1280

Luth WC (1976) Granitic rocks. In: Bailey DK, MacDonald R (eds), The Evolution of the Crystalline Rocks. Academic Press, London, pp 335–416

Malm OA, Ormaasen DE (1978) Mangerite charnockite intrusives in the Lofoten–Vesteralen area, north Norway: petrography, chemistry and petrology. Norges Geol Unders 338: 83–114

Middlemost EAK (1989) Iron oxidation ratios, norms and the classification of volcanic rocks. Chem Geol 77: 19–26

Middlemost EAK (1994) Naming materials in the magma/igneous rock system. Earth Sci Rev 37: 215–224

Moyen J-F, Janoušek V, Laurent O, Bachmann O, Jacob J-B, Farina F, Fiannacca P, Villaros A (2021) Crustal melting vs. fractionation of basaltic magmas: Part 1, granites and paradigms. Lithos 402–403: 106291

Nabelek PI (2020) Petrogenesis of leucogranites in collisional orogens. In: Janoušek V, Bonin B, Collins WJ, Farina F, Bowden P (eds) Post-Archaean Granitic Rocks: Contrasting Petrogenetic Processes and Tectonic Environments. Geological Society, London, Special Publications 491: 179–207

Peccerillo A (2017) Cenozoic Volcanism in the Tyrrhenian Sea Region, 2nd edition. Springer, Cham, pp 1–399

Poubová M (1974) Composition of amphiboles and rock type subdivisions in the Central Bohemian Pluton. Krystalinikum 10: 149–169

Rodríguez-García G, Zapata JP, Correa-Martínez AM, Sabrica C, Obando G (2022) Redefinición, correlación e implicaciones geotectónicas del batolito de Ibagué, Colombia (Redefinition, correlation and geotectonic implications of the batholith of Ibagué, Colombia). Boletín de Geol 44: 65–93

Stanley C (2017) Lithogeochemical classification of igneous rocks using Streckeisen ternary diagrams. Geochem: Explor Environ Anal 17: 63–91

Streckeisen A (1976) To each plutonic rock its proper name. Earth Sci Rev 12: 1–33

Streckeisen A L, Le Maitre RW (1979) Chemical approximation to modal QAPF classification of the igneous rocks. Neu Jb Mineral, Abh 136: 169–206

Tuttle OF, Bowen NL (1958) Origin of granite in the light of experimental studies in the system $NaAlSi_3O_8$–$KAlSi_3O_8$–SiO_2–H_2O. GSA Memoir 74, pp 1–145

Verma SP, Torres-Alvarado IS, Sotelo-Rodríguez ZT (2002) SINCLAS: standard igneous norm and volcanic rock classification system. Comput Geosci 28: 711–715

Vilinovič V, Petrík I (1982) Classification of granitoid rocks according to mesonorm. Geol Carpath 33: 147–157

Wang J, Li B, Zhou D, Yao S, Li Z (1994) Geological Characteristics of the Intermediate–Acid Plutons of Hebei Province and Their Relations to the Ore-Forming Processes. Geological Publishing House, Beijing, pp 1–213 (in Chinese)

Whalen JB, Frost CD (2013) The Q–ANOR diagram: a tool for the petrogenetic and tectonomagmatic characterization of granitic suites. Geological Society of America Conference: South-Central Section: Abstracts with Programs 45: 24

Weiss S, Troll G (1989) The Ballachulish Igneous Complex, Scotland: petrography, mineral chemistry, and order of crystallization in the monzodiorite–quartz diorite suite and in the granite. J Petrol 30: 1069–1115

Wolska A (2012) Petrology and geochemistry of granitoids and their mafic microgranular enclaves (MME) in marginal part of the Małopolska Block (S Poland). Mineralogia 43: 3–127